NASA TM X-56034

FLIGHT-DETERMINED STABILITY AND CONTROL DERIVATIVES FOR AN EXECUTIVE JET TRANSPORT

Harriet J. Smith

July 1975

NASA Flight Research Center
Edwards, California 93523

1. Report No.	2. Government Accession No.	3. Recipient's Catalog No.
NASA TM X-56034		

4. Title and Subtitle	5. Report Date
FLIGHT-DETERMINED STABILITY AND CONTROL DERIVATIVES FOR AN EXECUTIVE JET TRANSPORT	July 1975
	6. Performing Organization Code
7. Author(s)	8. Performing Organization Report No.
Harriet J. Smith	H-901
	10. Work Unit No.
9. Performing Organization Name and Address	505-06-91
NASA Flight Research Center P.O. Box 273 Edwards, California 93523	11. Contract or Grant No.
	13. Type of Report and Period Covered
12. Sponsoring Agency Name and Address	Technical Memorandum
National Aeronautics and Space Administration Washington, D.C. 20546	14. Sponsoring Agency Code

15. Supplementary Notes

16. Abstract

A modified maximum likelihood estimation (MMLE) technique which included a provision for including a priori information about unknown parameters was used to determine the aerodynamic derivatives of the Lockheed JetStar airplane.

Two hundred sixty-five maneuvers were performed with the JetStar airplane, which was modified to include direct lift controls, to obtain lateral-directional and longitudinal derivatives. Data were obtained at altitudes of 3048 meters, 6096 meters, and 9144 meters (10,000 feet, 20,000 feet, and 30,000 feet) and over an angle of attack range from approximately 3° to 13° and a Mach number range from 0.25 to 0.75. Side force generators were installed and tested in 87 maneuvers to determine their effectiveness and their effect on the other derivatives. Lateral-directional data for four flight conditions were analyzed without using a priori information to assess the effect of this feature on the results.

The MMLE method generally gave consistent (repeatable) estimates of the derivatives, with the exception of the rolling moment due to yaw rate, which showed large variances.

17. Key Words (Suggested by Author(s))	18. Distribution Statement
Stability and control derivatives JetStar airplane	Unclassified - Unlimited

19. Security Classif. (of this report)	20. Security Classif. (of this page)	21. No. of Pages	22. Price*
Unclassified	Unclassified	45	

FLIGHT-DETERMINED STABILITY AND CONTROL DERIVATIVES FOR AN EXECUTIVE JET TRANSPORT

Harriet J. Smith
Flight Research Center

INTRODUCTION

There is a continuing need for handling qualities investigators to have reliable estimates of stability and control derivatives for all types of airplanes. Obtaining these estimates has been difficult and time consuming; therefore, the NASA Flight Research Center developed a modified maximum likelihood estimation (MMLE) program (refs. 1 and 2) to make possible the rapid determination of airplane stability and control derivatives from flight data.

The MMLE program is currently being used to obtain stability and control derivatives for several airplanes. One of the aircraft for which this is being done is the Lockheed JetStar airplane, which is representative of medium size executive jet transports.

The airplane used in this investigation had been modified for airborne simulation (ref. 3) and was equipped with direct lift controls and removable side force generators; therefore, in addition to determining the usual stability and control derivatives, the effectiveness of these controls was evaluated. Lateral-directional and longitudinal derivatives were obtained with and without the side force generators installed.

Because of the large amount of data (for over 350 maneuvers), this study presented an opportunity for a realistic evaluation of the analysis technique, including the effects of using an optional feature (ref. 1) in which a priori information about the derivatives is used.

The tests were made over a Mach number range from 0.25 to 0.75 and at altitudes of 3048 meters, 6096 meters, and 9144 meters (10,000 feet, 20,000 feet, and 30,000 feet). Both longitudinal and lateral-directional maneuvers were performed with the basic aircraft and with the side force generators installed. This report presents the results of these tests and a comparison with wind-tunnel derivatives that were extracted from data presented in reference 4.

SYMBOLS

A	stability matrix
a_X	longitudinal acceleration, g
a_Y	lateral acceleration, g
a_Z	vertical acceleration, g
B	control matrix
b	wingspan, m (ft)
C	stability observation matrix
$\bar{c}$	wing mean aerodynamic chord, m (ft)
c	vector of unknown coefficients
c_0	vector of a priori estimates of the unknown coefficients
D	control observation matrix
D_1	weighting matrix for observation vector
D_2	weighting matrix for a priori estimate vector
$d_{1_{ii}}$	ith diagonal element in the D_1 matrix
$d_{2_{ii}}$	ith diagonal element in the D_2 matrix
h	altitude, m (ft)
i	row index
J	cost functional or weighted mean-square-fit error
K	scalar weighting factor (gain) for a priori weighting matrix
L	rolling moment divided by the moment of inertia about the longitudinal axis, rad/sec^2
M	pitching moment divided by the moment of inertia about the lateral axis, rad/sec^2

N	yawing moment divided by the moment of inertia about the vertical axis, rad/sec^2
p	roll rate, rad/sec
q	pitch rate, rad/sec
$\bar{q}$	dynamic pressure, N/m^2 (lb/ft^2)
r	yaw rate, rad/sec
S	wing area, m^2 (ft^2)
T	total time, sec
t	time, sec
u	control vector
V	velocity, m/sec (ft/sec)
X	longitudinal force divided by mass, m/sec^2 (ft/sec^2)
x	state vector
Y	side force divided by mass and velocity, rad/sec
y	observation vector
Z	normal force divided by mass and velocity, rad/sec
z	measurement of observation vector
α	angle of attack, rad or deg
α_0	angle of attack of principal axis, rad or deg
β	angle of sideslip, rad or deg
δ_a	aileron deflection, rad or deg
δ_{dlc}	direct lift control deflection, rad or deg
δ_e	elevator deflection, rad or deg
δ_r	rudder deflection, rad or deg
δ_{sfg}	side force generator deflection, rad or deg

δ_0 constant control deflection, rad or deg

θ pitch angle, rad or deg

σ standard deviation

φ bank angle, rad or deg

$\nabla_c( )$ gradient of ( ) with respect to c

Nondimensional coefficients:

C_L lift coefficient, $\frac{\text{Lift}}{\bar{q}S}$

$C_{L_\alpha} = \partial C_L/\partial\alpha$

$C_{L_{\alpha=0}}$ lift coefficient at $\alpha = 0$

$C_{L_{\delta_e}} = \partial C_L/\partial\delta_e$

$C_{L_{\delta_{dlc}}} = \partial C_L/\partial\delta_{dlc}$

C_l rolling-moment coefficient, $\frac{\text{Rolling moment}}{\bar{q}Sb}$

$C_{l_p} = \partial C_l/\partial pb/2V$

$C_{l_r} = \partial C_l/\partial rb/2V$

$C_{l_\beta} = \partial C_l/\partial\beta$

$C_{l_{\delta_a}} = \partial C_l/\partial\delta_a$

$C_{l_{\delta_r}} = \partial C_l/\partial\delta_r$

$C_{l_{\delta_{sfg}}} = \partial C_l/\partial\delta_{sfg}$

C_m pitching-moment coefficient, $\frac{\text{Pitching moment}}{\bar{q}S\bar{c}}$

$C_{m_q} = \partial C_m/\partial q\bar{c}/2V$

$C_{m_{\alpha=0}}$ pitching-moment coefficient at $\alpha = 0$

$C_{m_\alpha} = \partial C_m/\partial\alpha$

$C_{m_{\delta_e}} = \partial C_m/\partial\delta_e$

$C_{m_{\delta_{dlc}}} = \partial C_m/\partial\delta_{dlc}$

C_n yawing-moment coefficient, $\frac{\text{Yawing moment}}{\bar{q}Sb}$

$C_{n_p} = \partial C_n/\partial pb/2V$

$C_{n_r} = \partial C_n/\partial rb/2V$

$C_{n_\beta} = \partial C_n/\partial\beta$

$C_{n_{\delta_a}} = \partial C_n/\partial\delta_a$

$C_{n_{\delta_r}} = \partial C_n/\partial\delta_r$

$C_{n_{\delta_{sfg}}} = \partial C_n/\partial\delta_{sfg}$

C_y side force coefficient, $\frac{\text{Side force}}{\bar{q}S}$

$C_{y_\beta} = \partial C_y/\partial\beta$

$C_{y_{\delta_r}} = \partial C_y/\partial\delta_r$

$C_{y_{\delta_{sfg}}}$ = $\partial C_y / \partial \delta_{sfg}$

Subscript:

k iteration index

Superscript:

T transpose

A dot over a quantity denotes the time derivative of that quantity. Italic type indicates a vector.

DESCRIPTION OF AIRPLANE AND CONTROL SYSTEM

The Lockheed JetStar airplane is a medium range, swept-wing, executive jet transport airplane which is powered by four Pratt & Whitney JT12A-6A engines. Each wing contains two integral fuel tanks with a capacity of approximately 1450 liters (383 gallons) each. In addition, an externally mounted fuel tank with a capacity of approximately 2140 liters (565 gallons) is installed on each wing. Normally, each engine is supplied by its respective tank in flight; however, crossfeed is possible. The airplane's weight during these tests varied from approximately 15,945 kilograms (35,150 pounds) down to approximately 12,475 kilograms (27,500 pounds). The pertinent physical characteristics of the airplane are given in table 1. The JetStar airplane without side force generators is shown in figure 1, and a three-view drawing of the airplane with side force generators is shown in figure 2.

The JetStar airplane uses conventional aileron, rudder, and elevator control surfaces for lateral, directional, and longitudinal control. The ailerons and elevator are hydraulically boosted, with a boost ratio of 5.5 for the ailerons and 3.2 for the elevator. Rudder control is obtained through a direct cable-bell crank arrangement. Air loads on the rudder are reduced by means of a balance tab, which also serves as a rudder trim tab. An electrically driven screw jack actuator, which is controlled from a switch on the pedestal, is used to position the tab up to 9° left or right of neutral. The ailerons are trimmed similarly; an electric actuator positions a trim tab on the left aileron. The horizontal stabilizer is rigidly attached to the vertical fin, and the fin is attached to the fuselage by a pin through the fin's rear spar. A dual electromechanical actuator is mounted on the fuselage structure, with its screw jacks connected to the fin's front spar. Pitch trim is accomplished by rotating the entire tail assembly about the rear spar attachment fitting. The horizontal stabilizer is capable of moving 1° up or 4° down with wing flaps retracted and 9° down with flaps extended.

The JetStar airplane employs leading-edge flaps for reducing approach and landing speeds. There are four leading-edge flaps, two on each wing. The outboard flaps can be deflected 27°, and the inboard flaps can be deflected 22°. There are also four trailing-edge flaps, two for each wing; however, all four sections deflect a maximum of 50°.

The speed brake is faired into the bottom of the fuselage in back of the passenger compartment. Two hydraulic cylinders extend and retract the brake through an angle of 60°.

The airplane used in this investigation was also equipped with direct lift controls and removable side force generators (fig. 2). The direct lift controls consisted of two direct lift control tabs on each flap, which produce vertical loads; one tab was inboard and one was outboard of the wing's external tank. Two side force generators were mounted side by side beneath the center wing to produce lateral loads. Each side force generator was equipped with a trailing-edge tab that was geared to deflect 1.5 degrees per degree of side force generator deflection. The direct lift controls and the side force generator were manually operated by knobs on the pilot's control panel.

When the direct lift controls are not being used, they become an integral part of the normal flap system and have no effect on the airplane's characteristics. Therefore, for the tests reported herein, the airplane without side force generators installed is referred to as the basic airplane, even though the aircraft included direct lift controls.

TESTS

Three flights were flown with the aircraft without the side force generators installed. Flights were made at altitudes of 3048 meters, 6096 meters, and 9144 meters (10,000 feet, 20,000 feet, and 30,000 feet), and over an angle of attack range from approximately 3° to 13° and a Mach number range of 0.25 to 0.75. Table 2 shows the flight conditions at which the data were obtained.

For the longitudinal tests, two pulses in each direction were made with the elevator and the direct lift controls. In addition, four steps (two in each direction) of approximately 3 seconds' duration were made with the direct lift controls. In all, 12 longitudinal maneuvers were performed at each flight condition shown in table 2.

For the lateral-directional tests, four aileron doublets and four rudder doublets were performed at each flight condition. The longitudinal and lateral-directional maneuvers were repeated with the aircraft in the approach configuration (20° flap setting and gear down) at 149 knots indicated airspeed (KIAS) at the 3048-meter (10,000-foot) flight condition. In total, the flight plan for the aircraft without the side force generators called for 260 maneuvers. Because of repetitions, 265 maneuvers were actually performed.

After the completion of the flight program with the basic JetStar airplane, the side force generators were installed. The purpose of the investigation with the side force generators was twofold: (1) to determine the effect of the side force generators on the aerodynamic characteristics of the airplane, and (2) to determine the control effectiveness of the side force generators. Inasmuch as the first requirement was met with the aileron and rudder doublets, the side force generator maneuvers were performed primarily for the purpose of determining their effectiveness. Therefore, in

addition to single side force generator pulses, a series of pulses of approximately 15 seconds' total duration was performed with the side force generators.

Although the presence of the side force generators was not expected to affect the longitudinal characteristics of the aircraft, longitudinal maneuvers were performed at a few of the flight conditions to confirm this assumption. In all, 87 maneuvers were performed with the side force generators installed. The flight conditions at which data were obtained with side force generators installed are indicated in table 2.

METHOD OF ANALYSIS

The MMLE method used in this investigation has been referred to as quasilinearization, or the modified Newton-Raphson technique. The method is described in detail in reference 1 and is only summarized herein.

The model used to describe the dynamics of the aircraft is as follows:

$$\dot{x} = Ax + Bu \tag{1}$$

$$y = Cx + Du \tag{2}$$

where the lateral-directional state and control vectors are

$$x = (p\ r\ \beta\ \varphi)^T$$

$$u = (\delta_a\ \delta_r\ \delta_{sfg}\ \delta_0)^T$$

and the longitudinal state and control vectors are

$$x = (q\ \alpha\ V\ \theta)^T$$

$$u = (\delta_e\ \delta_{dlc}\ \delta_0)^T$$

The lateral-directional observation vector is

$$y = (p\ r\ \beta\ \varphi\ \dot{p}\ \dot{r}\ a_Y)^T$$

and the longitudinal observation vector is

$$y = (q\ \alpha\ V\ \theta\ \dot{q}\ a_Z\ a_X)^T$$

The lateral-directional state and control matrices are

$$A = \begin{bmatrix} L_p & L_r & L_\beta & 0 \\ N_p & N_r & N_\beta & 0 \\ \alpha_0 & -1 & Y_\beta & Y_\varphi \\ 1 & 0 & 0 & 0 \end{bmatrix} \qquad B = \begin{bmatrix} L_{\delta_a} & L_{\delta_r} & L_{\delta_{sfg}} & L_{\delta_0} \\ N_{\delta_a} & N_{\delta_r} & N_{\delta_{sfg}} & N_{\delta_0} \\ Y_{\delta_a} & Y_{\delta_r} & Y_{\delta_{sfg}} & Y_{\delta_0} \\ 0 & 0 & 0 & 0 \end{bmatrix}$$

and the longitudinal state and control matrices are

$$A = \begin{bmatrix} M_q & M_\alpha & M_V & 0 \\ Z_q & Z_\alpha & Z_V & Z_\theta \\ X_q & X_\alpha & X_V & X_\theta \\ 1 & 0 & 0 & 0 \end{bmatrix} \qquad B = \begin{bmatrix} M_{\delta_e} & M_{\delta_{dlc}} & M_{\delta_0} \\ Z_{\delta_e} & Z_{\delta_{dlc}} & Z_{\delta_0} \\ X_{\delta_e} & X_{\delta_{dlc}} & X_{\delta_0} \\ 0 & 0 & 0 \end{bmatrix}$$

The lateral-directional observation matrices are

$$C = \begin{bmatrix} 1 & 0 & 0 & 0 \\ 0 & 1 & 0 & 0 \\ 0 & 0 & 1 & 0 \\ 0 & 0 & 0 & 1 \\ L_p & L_r & L_\beta & 0 \\ N_p & N_r & N_\beta & 0 \\ 0 & 0 & Y_\beta & 0 \end{bmatrix} \qquad D = \begin{bmatrix} 0 & 0 & 0 & 0 \\ 0 & 0 & 0 & 0 \\ 0 & 0 & 0 & 0 \\ 0 & 0 & 0 & 0 \\ L_{\delta_a} & L_{\delta_r} & L_{\delta_{sfg}} & L_{\delta_0} \\ N_{\delta_a} & N_{\delta_r} & N_{\delta_{sfg}} & N_{\delta_0} \\ Y_{\delta_a} & Y_{\delta_r} & Y_{\delta_{sfg}} & Y_{\delta_0} \end{bmatrix}$$

and the longitudinal observation matrices are

$$C = \begin{bmatrix} 1 & 0 & 0 & 0 \\ 0 & 1 & 0 & 0 \\ 0 & 0 & 1 & 0 \\ 0 & 0 & 0 & 1 \\ M_q & M_\alpha & M_V & 0 \\ 0 & Z_\alpha & 0 & 0 \\ 0 & X_\alpha & 0 & 0 \end{bmatrix} \qquad D = \begin{bmatrix} 0 & 0 & 0 \\ 0 & 0 & 0 \\ 0 & 0 & 0 \\ 0 & 0 & 0 \\ M_{\delta_e} & M_{\delta_{dlc}} & M_{\delta_0} \\ Z_{\delta_e} & Z_{\delta_{dlc}} & Z_{\delta_0} \\ X_{\delta_e} & X_{\delta_{dlc}} & X_{\delta_0} \end{bmatrix}$$

The cost functional to be minimized is:

$$J = \int_0^t \left[z(t) - y(t)\right]^T D_1 \left[z(t) - y(t)\right] dt \tag{3}$$

where $z(t)$ represents the actual measurements, $y(t)$ the model observation, and D_1 the diagonal observation weighting matrix. The D_1 matrix was selected to make the fit errors for each parameter approximately one.

When there is linear dependence between the effect of two or more derivatives, or when there is little or no information in the measurements for determining a derivative, the matrices become ill conditioned, and large differences can be obtained in the derivatives without significantly affecting the cost functional. When this occurs, it is sometimes advantageous to include in the cost functional a penalty for deviating from some a priori value assumed for the derivative.

The cost functional then becomes:

$$J = \int_0^t \left[z(t) - y(t)\right]^T D_1 \left[z(t) - y(t)\right] dt + (c - c_0)^T K D_2 (c - c_0) \tag{4}$$

where c_0 is the vector of a priori estimates of c and D_2 is the diagonal a priori weighting matrix. At first, wind-tunnel data were used for c_0; however, after the tests with the basic aircraft were completed, the a priori information was updated for the side force generator tests to reflect the differences between wind-tunnel and flight-test measurements. The result of using this modified cost functional is to reduce the scatter in the estimates when insufficient information exists to determine good estimates; however, the a priori weighting should not be so large as to drive the values of the derivatives to the a priori values when there is sufficient information to make good estimates. The weighting of the elements of the a priori weighting matrix depends on the variances of the a priori estimates; an overall weighting factor, K, was chosen that approximately doubled the fit error.

After several computer runs were made to select the appropriate D_1 and D_2 weighting matrices, each maneuver was analyzed without changing these weighting matrices. The values used in this experiment for the D_1 matrices are given in table 3, and the values used in the D_2 matrices are given in table 4.

RESULTS AND DISCUSSION

Lateral-Directional Stability and Control Derivatives

Fifty-two rudder doublets and 47 aileron doublets were analyzed by the MMLE technique to determine the lateral-directional stability derivatives at 12 flight conditions.

Two time histories are shown in figure 3. Figure 3(a) is a typical computer plot of an aileron doublet. A similar plot of a rudder doublet is presented in figure 3(b). These cases were analyzed with the a priori option. The results of combining the data for the same two maneuvers and analyzing them as one case without using the a priori option are shown in figure 4. It should be pointed out that if a rudder maneuver or an aileron maneuver is analyzed separately it is necessary to either use the a priori option or hold constant those derivatives that are associated with the control that is not disturbed.

There is no appreciable difference between the matches obtained with and without the a priori option; the fit for all the time histories is good except for the roll and yaw accelerations, and these quantities had zero weighting (table 3). The time history matches shown in figures 3 and 4 are representative of the lateral-directional matches that were obtained.

The lateral-directional stability and control derivatives are plotted in figure 5 as a function of angle of attack. The data presented in this figure are the mean and standard deviations for all the derivatives obtained at each flight condition. Typically, the control derivatives represent four maneuvers and all the other derivatives represent eight, since the derivatives obtained from the rudder and the aileron maneuvers were averaged. The vertical lines around the symbols represent one standard deviation; where none is shown, the standard deviation is less than the height of the symbol. The four flight conditions denoted by the solid symbols were analyzed by combining the rudder and aileron maneuvers and omitting the a priori option. In the approach configuration, the flaps were deflected 20° and the gear were down.

The results presented in figure 5(a) show the MMLE estimates of C_{l_β}, C_{n_β}, and C_{y_β} to be consistent, which is indicated by the low variances, and also different from the wind-tunnel measurements. The estimates of C_{l_β} agree with the wind-tunnel measurements at the lower angles of attack; however, the wind-tunnel measurements indicate an increase in dihedral with angle of attack that is not confirmed by the MMLE analysis of the flight data. The estimates of C_{n_β} and C_{y_β} are lower

than the wind-tunnel predictions throughout the angle-of-attack range. At the four conditions where the estimates were obtained without using the a priori option, the variances are not significantly greater and the estimates of C_{l_β} and C_{n_β} are virtually the same as those obtained by using the a priori option. The estimates of C_{y_β} are somewhat lower and further removed from the wind-tunnel measurements when the combined maneuvers were analyzed and the a priori option was not used. This might indicate that the a priori weighting on C_{y_β} was too high. This possibility was investigated by varying the a priori weighting on the C_{y_β} derivative at one flight condition. The estimates of C_{y_β} obtained from aileron maneuvers did change when the a priori weighting was reduced, and there was considerable scatter in the estimates. The rudder maneuvers, however, gave consistent estimates of C_{y_β} with or without the use of the a priori option. The C_{l_β} and C_{n_β} estimates were also slightly more consistent when determined from rudder pulses than when determined from aileron pulses. Therefore, it is assumed that the best possible estimates of the β derivative are those obtained from rudder maneuvers; these estimates are given in figure 6.

The control derivatives (figs. 5(b) and 5(c)) show the same trend as the stability derivatives shown in figure 5(a). Again, the MMLE estimates are consistent and lower than the wind-tunnel measurements. In addition, the estimates obtained from the combined maneuvers without the a priori option are generally the same as those obtained with the option with the exception of the $C_{l_{\delta_r}}$ estimates at the two lowest angles of attack. At these two conditions the analyses of the combined maneuvers without the a priori option gave poor estimates, as evidenced by the large variances. Inasmuch as the estimates obtained by using the a priori option were significantly different from the wind-tunnel data, it did not appear that the a priori weighting on $C_{l_{\delta_r}}$ was too large. For this reason and because the variances were not large, it appeared that the original analysis with the a priori option resulted in reliable estimates of $C_{l_{\delta_r}}$. However, to resolve these differences, some of the data were analyzed again using different a priori weightings on some of the parameters. It was determined from this additional analysis that the discrepancy in the estimates was caused by including aileron maneuvers in the combined maneuver analysis and was not due to any effect of using a priori information in the analysis.

The rotary derivatives (fig. 5(d)) are usually more difficult to estimate, and this is confirmed by the higher variances shown here. The yawing moment due to roll rate, C_{n_p}, appears to be an exception; the estimates obtained without using the a priori option agreed well with those obtained using the option.

The estimates of C_{n_r} closely matched the wind-tunnel data when the a priori op-

tion was used and were generally greater when the a priori option was not used; however, the variances were significantly larger. To a lesser extent, the C_{l_p} estimates exhibit the same characteristics. This would indicate that insufficient information existed in the data to determine these derivatives accurately. The same is true of C_{l_r}, the only difference being that higher a priori weightings on C_{n_r} and C_{l_p} tended to make them match the wind-tunnel data; the C_{l_r} estimates were approximately the same with or without using a priori information in the analysis and had large variances.

Longitudinal Stability and Control Derivatives

The longitudinal stability and control derivatives are presented in figure 7 as a function of Mach number. The lift-curve slope and pitching moment due to angle of attack are presented in figure 7(a). The lift-curve slope agrees fairly well with the wind-tunnel data, although it is slightly higher throughout the Mach number range. The values of C_{m_α} obtained from flight are also consistently higher than the wind-tunnel data.

Lift- and pitching-moment coefficients for zero angle of attack are presented in figure 7(b). Both of these parameters agree fairly well with wind-tunnel estimates at the higher Mach numbers, but they do not agree well at the lower Mach numbers. However, the high variances of the $C_{L_{\alpha=0}}$ estimates for the lower Mach numbers indicated that these estimates were relatively poor.

The elevator control effectiveness is presented in figure 7(c) as a function of Mach number. The lift due to elevator agrees fairly well with wind-tunnel estimates above a Mach number of approximately 0.4. At the lower Mach numbers the flight-determined estimates appear slightly lower; however, because of the large variances of these estimates it is uncertain whether these differences are significant. The pitching-moment derivatives determined from flight are mostly larger than the wind-tunnel estimates; moreover, the flight data show an angle-of-attack effect at the higher Mach numbers that was not predicted by the wind-tunnel measurements (the lower the altitude, the lower the angle of attack for a given Mach number).

Direct lift control derivatives are shown in figure 7(d). The direct lift controls are approximately 20 percent more effective when deflected in the positive direction. This nonlinearity in lift effectiveness of the direct lift controls was also predicted by the wind-tunnel measurements; however, the magnitude of the flight $C_{L_{\delta_{dlc}}}$ is less than predicted by the wind tunnel. The lift effectiveness of the direct lift controls is approximately equal to that of the elevators; the only significant difference between the two controls is the pitching moment they produce. Although no pitching moment due to the direct lift controls was predicted by the wind-tunnel data, the flight measurements showed a small but significant pitching moment which increased with

increasing Mach number.

Figure 7(e) presents the pitch damping derivative, C_{m_q}. The flight-determined estimates of C_{m_q} are significantly larger than the wind-tunnel estimates.

Effect of Side Force Generators

Lateral-directional stability and control derivatives were obtained at five flight conditions with the side force generators installed. These derivatives are presented in figure 8 with the basic aircraft derivatives shown for comparison. The stability derivatives C_{l_β}, C_{n_β}, and C_{y_β} are shown in figure 8(a). The installation of the side force generators resulted in an increase in the lateral-directional stability of the aircraft. All three derivatives were significantly affected by the side force generators at the two lower angles of attack. The side force generators cause increases of approximately 100 percent, 60 percent, and 50 percent in C_{l_β}, C_{n_β}, and C_{y_β}, respectively. At the higher angles of attack the effects on C_{l_β} and C_{y_β} are considerably diminished, and there is no effect on C_{n_β}.

Control derivatives are shown in figures 8(b) and 8(c). In general, the control derivatives exhibited a similar trend with angle of attack, except for $C_{n_{\delta_a}}$. The increases, which occur in nearly all the derivatives at the lower angles of attack, appear to be a significant effect of the side force generators.

With the exception of C_{n_p}, the rotary derivatives for the aircraft with side force generators installed (fig. 8(d)) are also higher than the values obtained for the basic aircraft. The estimates for C_{l_r} and C_{n_r} have extremely large variances, so it is not known how significant these increases are; however, the mean values are consistently higher. The C_{l_p} estimates exhibit the same characteristics at the lower angles of attack, as noted previously.

The data in figure 8 were obtained from aileron, rudder, and side force generator doublets. To estimate side force generator effectiveness, series of side force generator pulses were analyzed in addition to the doublets. These series were approximately 15 seconds in duration; a sample time history is shown in figure 9.

No differences were observed in the control derivatives obtained from the two types of maneuvers, and the results, which are shown in figure 10, are the average of the estimates from all the side force generator maneuvers. The wind-tunnel estimates are for two angles of attack. The flight side force coefficients agree well with the wind-tunnel estimates, and the yawing and rolling moments due to the side force

generators are nearly zero, as predicted by the wind-tunnel data.

Longitudinal maneuvers were performed at three flight conditions with the side force generators installed (table 2). The derivatives obtained from these maneuvers were the same as those for the basic airplane within the standard deviation shown for each derivative in figure 7.

CONCLUSIONS

A modified maximum likelihood estimation technique that included a provision for including a priori information about unknown parameters was used to determine the aerodynamic coefficients of the Lockheed JetStar airplane from flight data. The aircraft used in this investigation was modified to include direct lift controls and removable side force generators. Derivatives were obtained with and without the side force generators installed. Two hundred sixty-five maneuvers were performed without the side force generators installed, and 87 additional maneuvers were performed with the side force generators installed.

The modified maximum likelihood estimation method generally gave consistent results for the lateral-directional stability and control derivatives; however, variances in the estimates of rolling moment due to yaw rate, C_{l_r}, were large.

The airplane's directional stability, C_{n_β}; side force coefficient, C_{y_β}; and lateral-directional control effectiveness, $C_{l_{\delta_a}}$ and $C_{n_{\delta_r}}$, were all lower than the wind-tunnel predictions.

More reliable estimates of C_{y_β} were obtained from rudder pulses than from aileron pulses.

The pitching-moment derivatives due to control deflection and pitching velocity, $C_{m_{\delta_e}}$ and C_{m_q}, are generally higher than the wind-tunnel estimates.

The flight-determined direct lift control derivatives confirmed the nonlinearity predicted from wind-tunnel tests. The direct lift control is more effective in the positive direction; however, the magnitude of the direct lift control effectiveness is less than indicated by the wind-tunnel predictions. In addition, the flight results showed that the direct lift controls exhibited some pitching moment.

The presence of the side force generators increased the estimates of C_{n_β}, C_{y_β}, and rolling moment due to sideslip, C_{l_β}, particularly at the lower angles of attack. The same effect was observed for the rotary derivatives and the aileron and rudder

derivatives, except for yawing moment due to aileron, $C_{n_{\delta_a}}$, and yawing moment due to roll rate, C_{n_p}.

Side force generator effectiveness agreed well with wind-tunnel estimates.

Flight Research Center
National Aeronautics and Space Administration
Edwards, California 93523
July 24, 1975

REFERENCES

1. Iliff, Kenneth W.; and Taylor, Lawrence W., Jr.: Determination of Stability Derivatives From Flight Data Using a Newton-Raphson Minimization Technique. NASA TN D-6579, 1972.

2. Maine, Richard E.; and Iliff, Kenneth W.: A FORTRAN Program for Determining Aircraft Stability and Control Derivatives From Flight Data. NASA TN D-7831, 1975.

3. Berry, Donald T.; and Deets, Dwain A.: Design, development, and utilization of a general purpose airborne simulator. AGARD Rept. 529, May 1966.

4. Clark, Daniel C.; and Kroll, John: General Purpose Airborne Simulator - Conceptual Design Report. NASA CR-544, 1966.

TABLE 1. - JETSTAR PHYSICAL CHARACTERISTICS

Wing -	
Area, m^2 (ft^2)	50.4 (542.5)
Span, m (ft)	16.36 (53.67)
Sweepback at 25-percent chord, deg	30
Aspect ratio	5.27
Mean aerodynamic chord, m (in.)	3.33 (131.2)
Dihedral angle, deg	0
Incidence angle of root chord, deg	1
Incidence angle of construction tip, deg	-1
Aileron -	
Area (rear of hinge line total), m^2 (ft^2)	2.26 (24.38)
Span, percent of wingspan	28
Chord, percent of wing chord without extension	25
Deflection, deg:	
Up	22
Down	17
Leading-edge flaps -	
Area forward of hinge line, m^2 (ft^2)	3.16 (34)
Span, percent of wingspan	53.5
Flap, percent local chord without extension	8
Hinge line, percent of local chord without extension	12
Maximum deflection, deg	27
Trailing-edge flaps (single slotted) -	
Area (extended), m^2 (ft^2)	5.82 (62.6)
Span, percent of wingspan	45.5
Chord, percent of wing chord	25
Maximum deflection, deg	50
Horizontal tail -	
Area, m^2 (ft^2)	13.84 (149)
Span, m (in.)	7.54 (297)
Chord at root, m (in.)	2.79 (110)
Chord at construction tip, m (in.)	0.91 (36)
Mean aerodynamic chord, m (in.)	2.01 (79.3)
Sweep at 25-percent chord, deg	30
Aspect ratio	4.03
Horizontal stabilizer -	
Area, m^2 (ft^2)	10.94 (117.8)
Span, m (ft)	7.56 (24.8)
Trim, deg:	
Nose up	1
Nose down	9

TABLE 1. - Concluded

Elevators -	
Area aft of hinge line, total, m^2 (ft^2)	2.90 (31.2)
Deflection (stops at booster), deg:	
Up	20
Down	16
Vertical tail -	
Area, m^2 (ft^2)	10.24 (110.2)
Span (water line 267), m (in.)	3.78 (149)
Chord at root, m (in.)	3.94 (155)
Chord at construction tip, m (in.)	1.47 (58)
Mean aerodynamic chord, m (in.)	2.89 (113.8)
Aspect ratio	1.4
Rudder -	
Area, m^2 (ft^2)	1.53 (16.45)
Deflection, deg	±30
Speed brake -	
Area, m^2 (ft^2)	0.85 (9.17)
Direct lift control -	
Area (inboard), m^2 (ft^2)	0.55 (5.94)
Area (outboard), m^2 (ft^2)	0.97 (10.46)
Mean aerodynamic chord, percent of span	28
Deflection, deg	±31
Side force generators -	
Area, total, m^2 (ft^2)	2.55 (27.44)
Mean aerodynamic chord, m (in.)	1.78 (70)
Deflection, deg:	
At 180 KIAS	22
At 240 KIAS	15.3
Fuselage -	
Length, m (ft)	18.41 (60.4)
Diameter (maximum), m (in.)	2.16 (85)
Maximum frontal area, m^2 (ft^2)	3.75 (40.4)
Height, m (ft)	6.22 (20.4)
Maximum certification weight, N (lb)	182,026 (40,921)

TABLE 2. - TEST FLIGHT CONDITIONS

Test	Mach number	Altitude, m (ft)	α, deg
1[a]	0.25	3048 (10,000)	12.5
2[b]	0.32	3048 (10,000)	9.1
3[b]	0.40	3048 (10,000)	6.1
4[c]	0.55	3048 (10,000)	3.0
5	0.32	6096 (20,000)	11.7
6[b]	0.40	6096 (20,000)	7.9
7	0.55	6096 (20,000)	4.4
8	0.65	6096 (20,000)	3.0
9	0.40	9144 (30,000)	11.1
10	0.55	9144 (30,000)	6.4
11	0.65	9144 (30,000)	4.6
12	0.75	9144 (30,000)	3.2

[a]The tests were repeated at this condition in the approach configuration (gear down, 20° flaps).

[b]Both longitudinal and lateral-directional maneuvers were performed with side force generators installed at these conditions.

[c]Only lateral-directional maneuvers were performed with side force generators installed at this condition.

TABLE 3. - VALUES USED IN THE OBSERVATION WEIGHTING MATRICES

Longitudinal			Lateral-directional		
i	y_i	$d_{1_{ii}}$	i	y_i	$d_{1_{ii}}$
1	q	364,000	1	β	450,000
2	α	571,000	2	p	66,300
3	V	0	3	r	1,410,000
4	θ	2,000,000	4	φ	86,100
5	$\dot{q}$	0	5	a_Y	19,100
6	a_Z	6,300	6	$\dot{p}$	0
7	a_X	0	7	$\dot{r}$	0

TABLE 4. - VALUES USED IN THE A PRIORI WEIGHTING MATRICES

(a) Longitudinal

i	C_i	$d_{2_{ii}}$
1	Z_{δ_e}	26,000
2	$Z_{\delta_{dlc}}$	200
3	Z_α	26,000
4	M_{δ_e}	30
5	$M_{\delta_{dlc}}$	0
6	M_α	30
7	M_q	1,600

TABLE 4. - Concluded

(b) Lateral-directional

i	C_i	$d_{2_{ii}}$
1	L_{δ_a}	1
2	L_{δ_r}	2
3	L_{δ_0}	0
4	L_p	5,000
5	L_r	500
6	L_β	10
7	N_{δ_a}	1,500
8	N_{δ_r}	1,500
9	N_{δ_0}	0
10	N_p	75,000
11	N_r	75,000
12	N_β	150
13	Y_{δ_a}	0
14	Y_{δ_r}	0
15	Y_{δ_0}	0
16	Y_p	130,000
17	Y_β	130,000

E-21742

Figure 1. JetStar airplane.

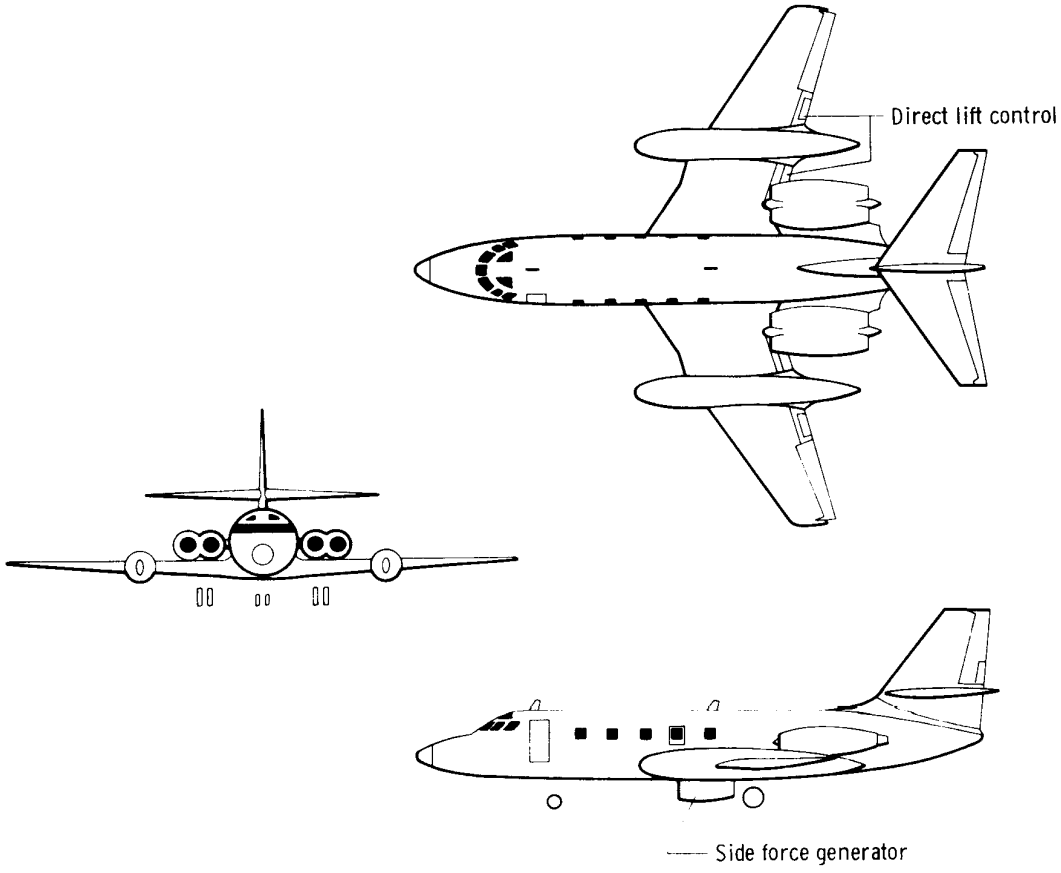

Figure 2. Three-view drawing of JetStar airplane.

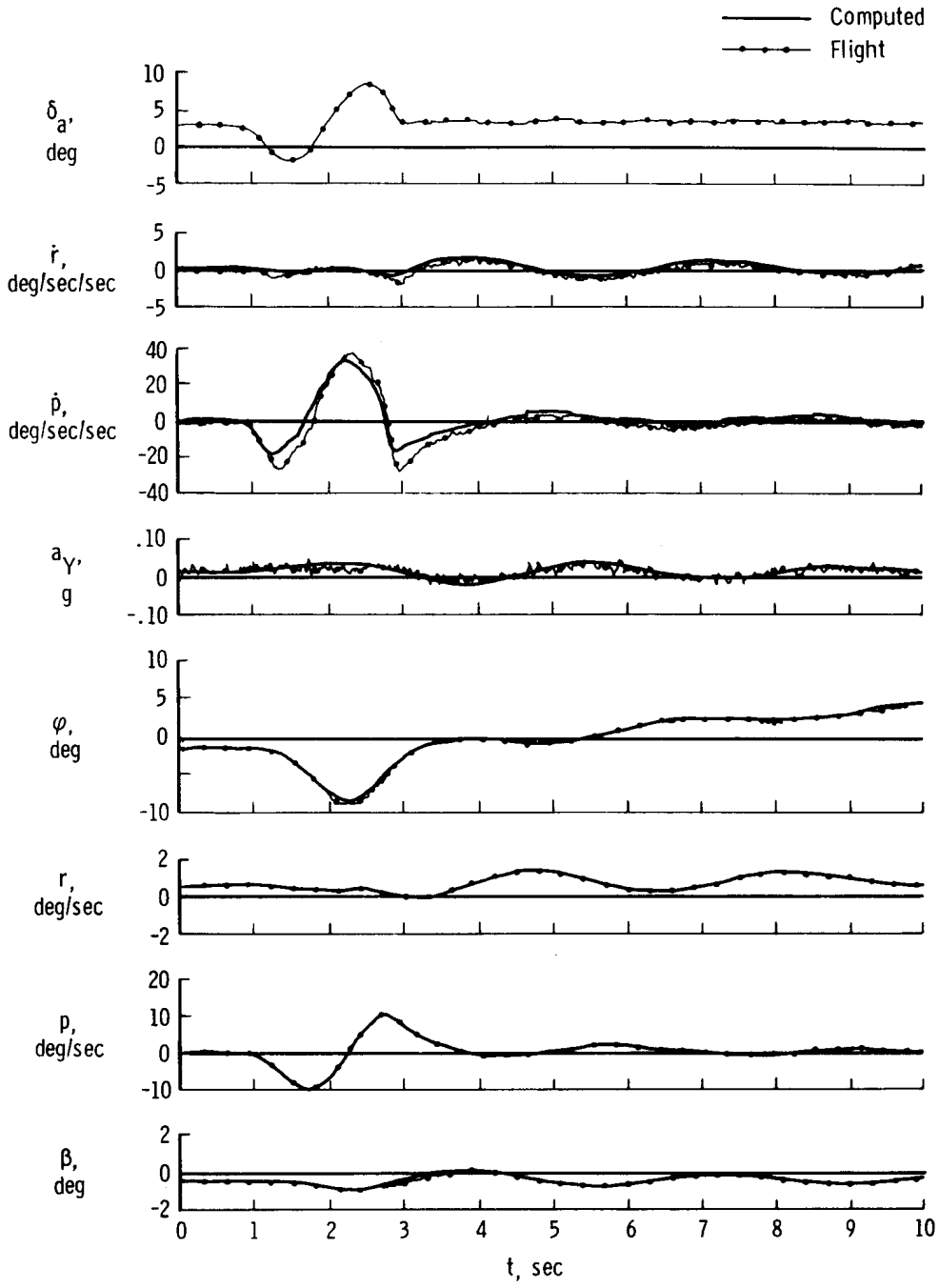

(a) δ_a doublet.

Figure 3. Comparison of time histories measured in flight and computed using derivatives determined from single (δ_a or δ_r) maneuver.

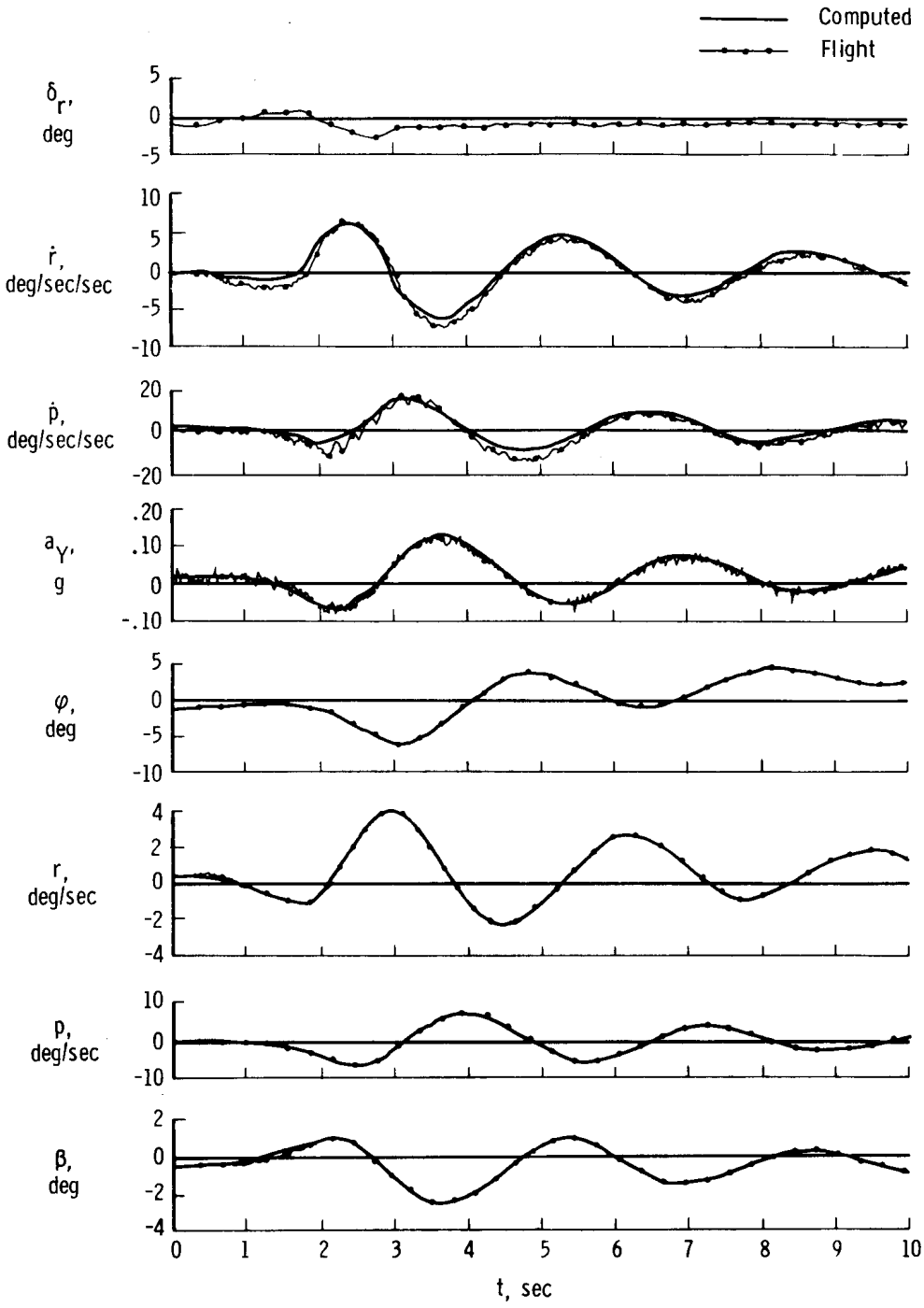

(b) δ_r doublet.

Figure 3. Concluded.

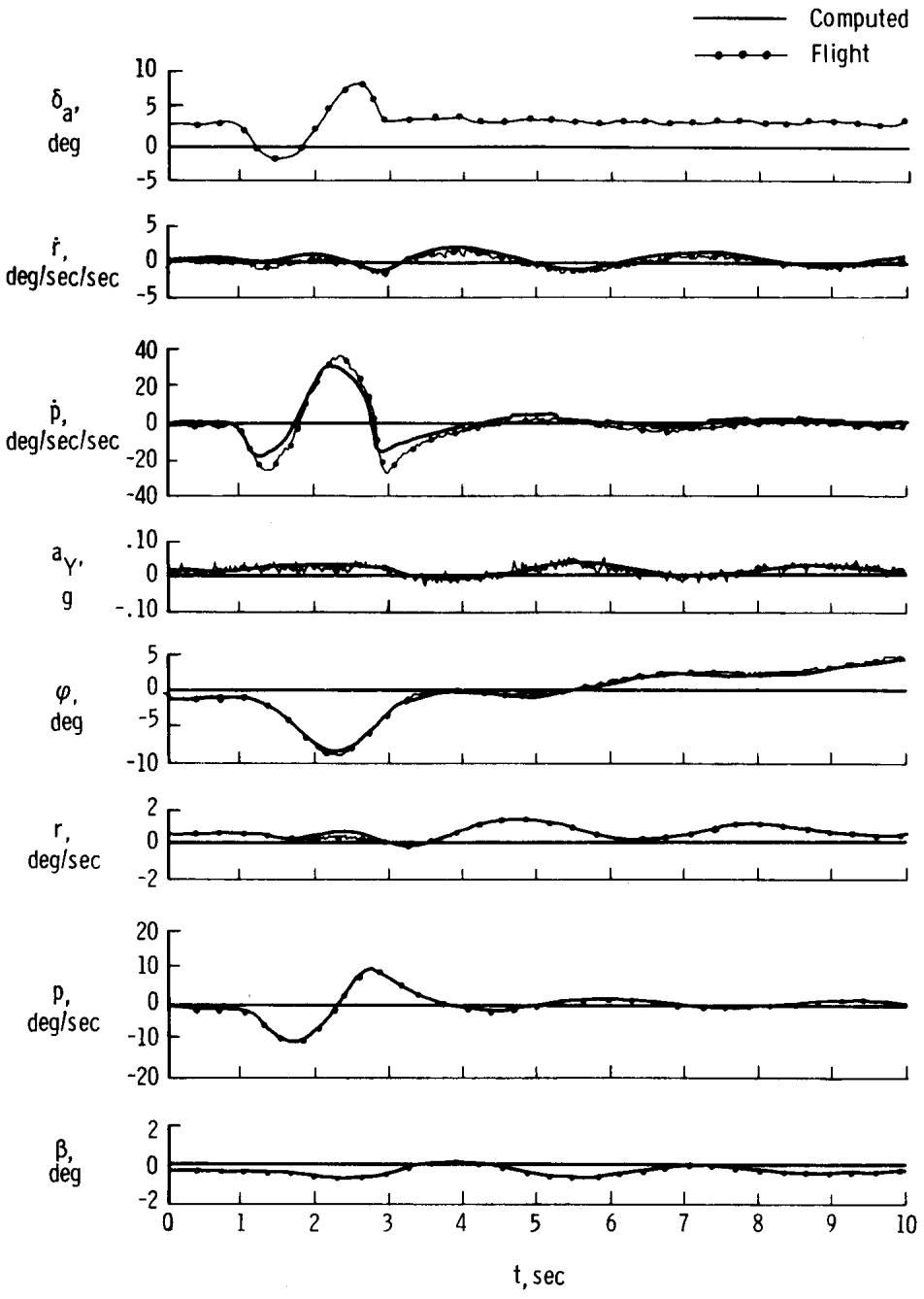

(a) δ_a doublet.

Figure 4. Comparison of time histories measured in flight and computed using derivatives determined from combined δ_a and δ_r maneuvers.

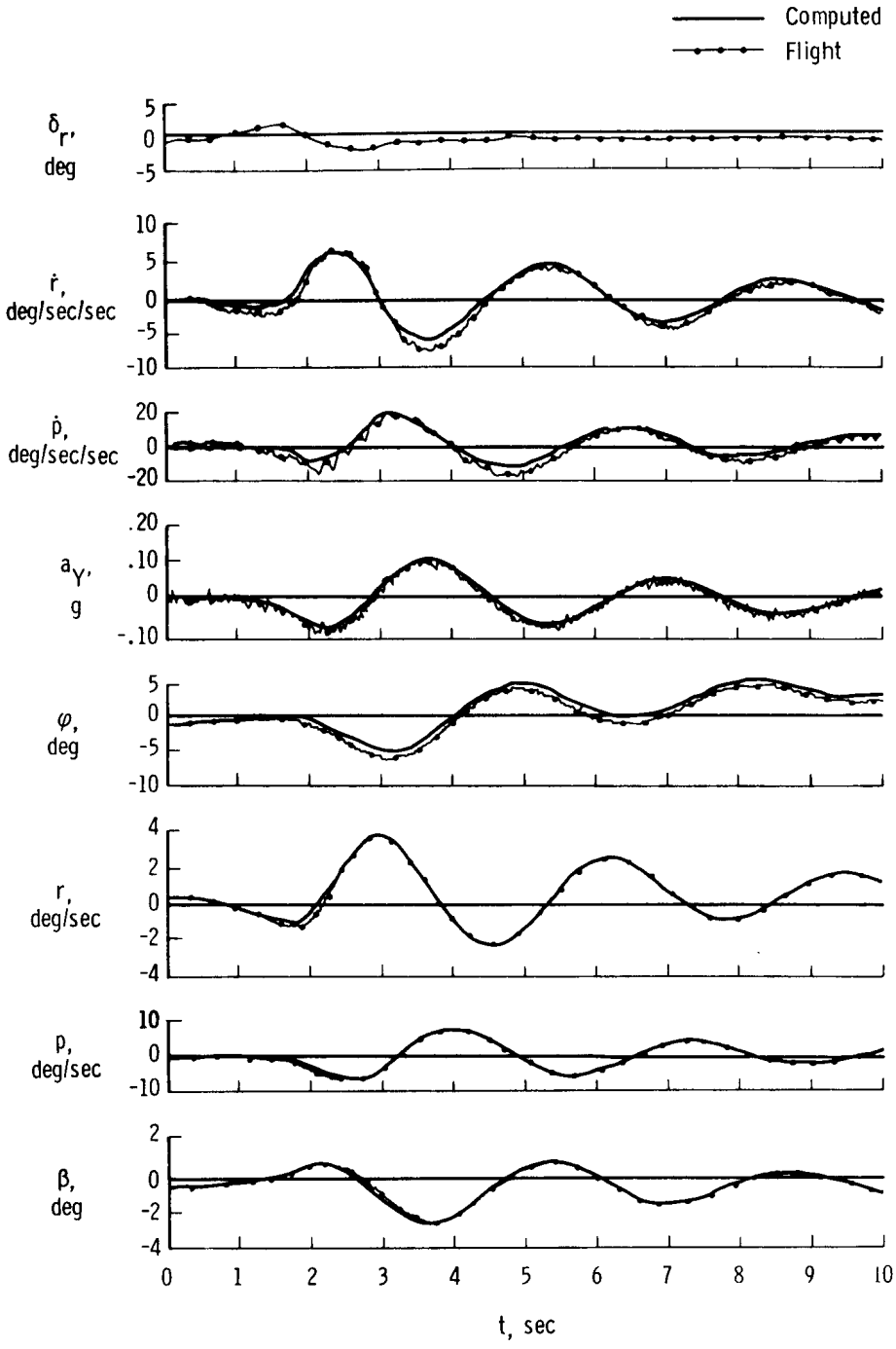

(b) δ_r doublet.

Figure 4. Concluded.

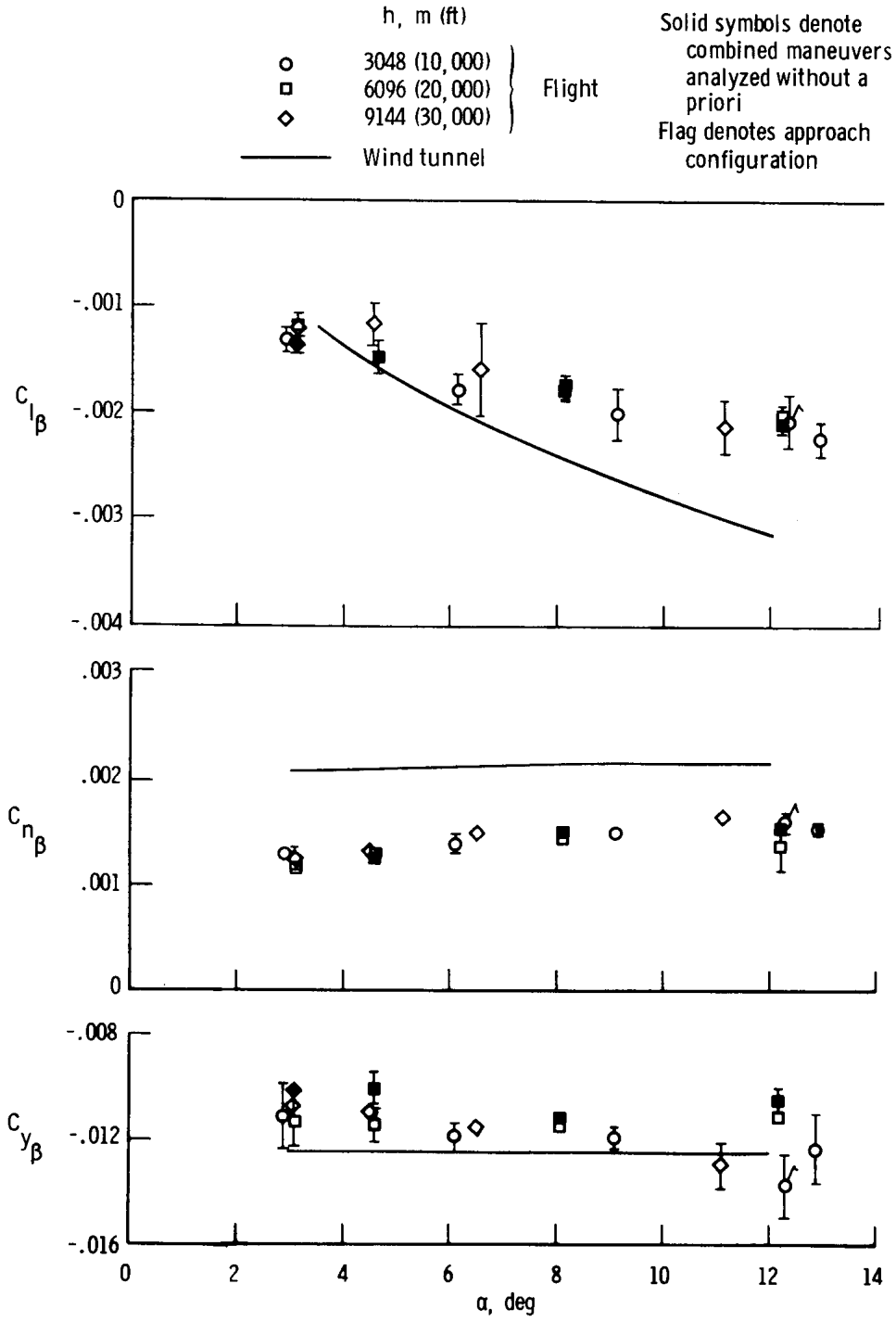

(a) β derivatives (preliminary).

Figure 5. Lateral-directional and control derivatives of the JetStar airplane obtained from flight by using the MMLE method.

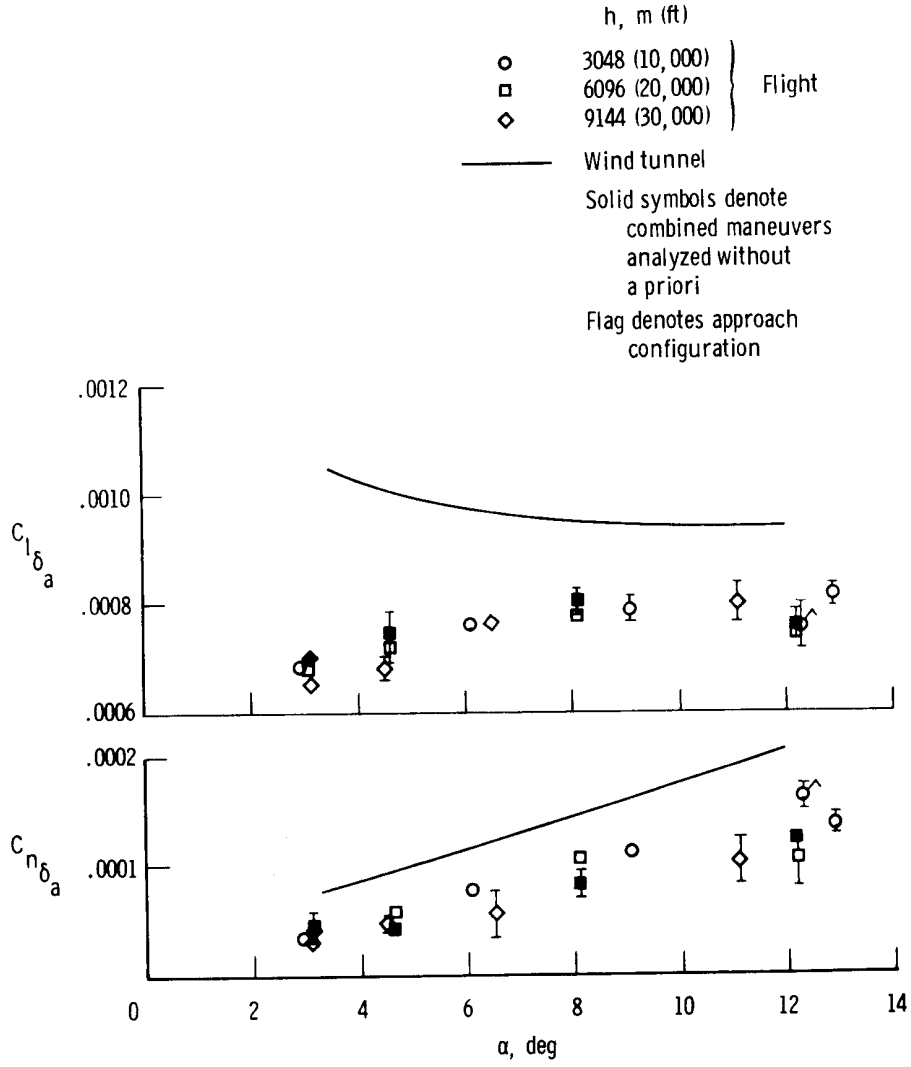

(b) δ_a derivatives.

Figure 5. Continued.

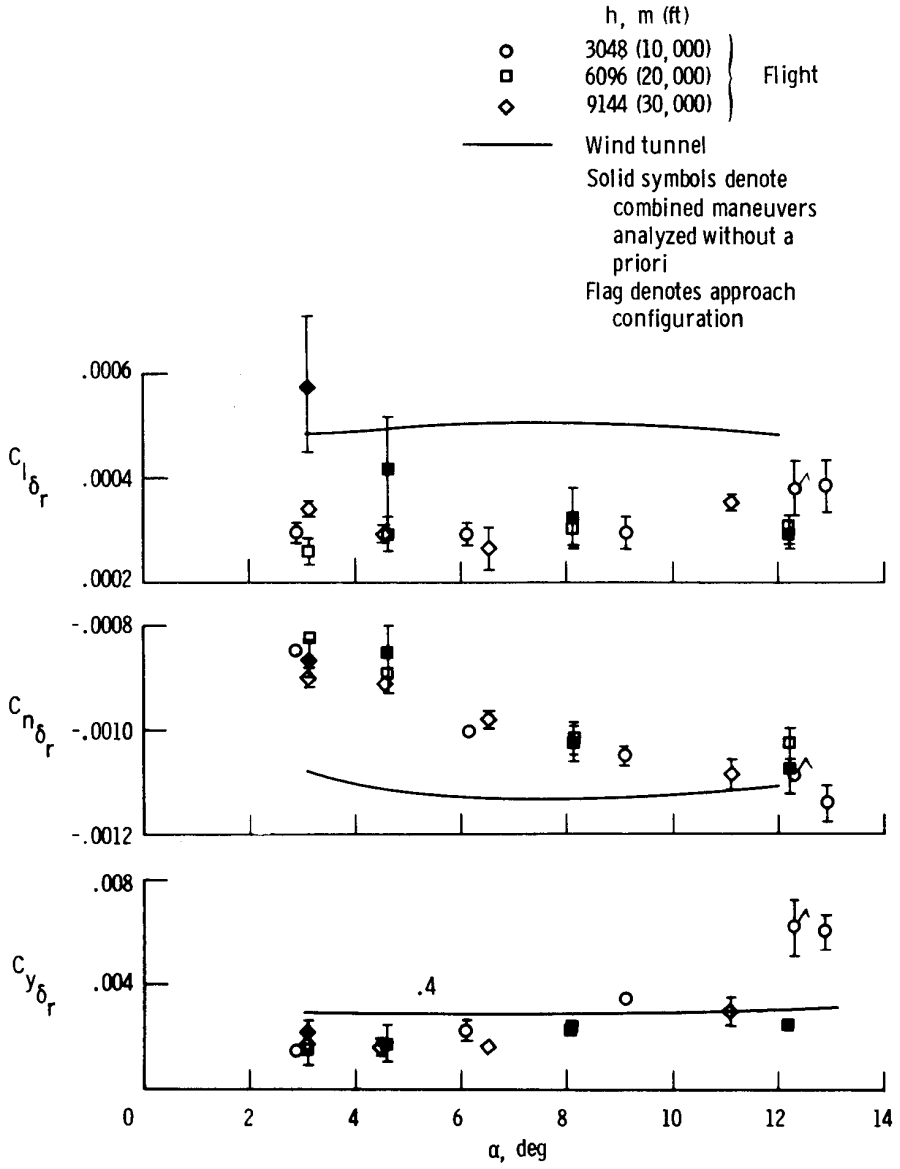

(c) δ_r derivatives.

Figure 5. Continued.

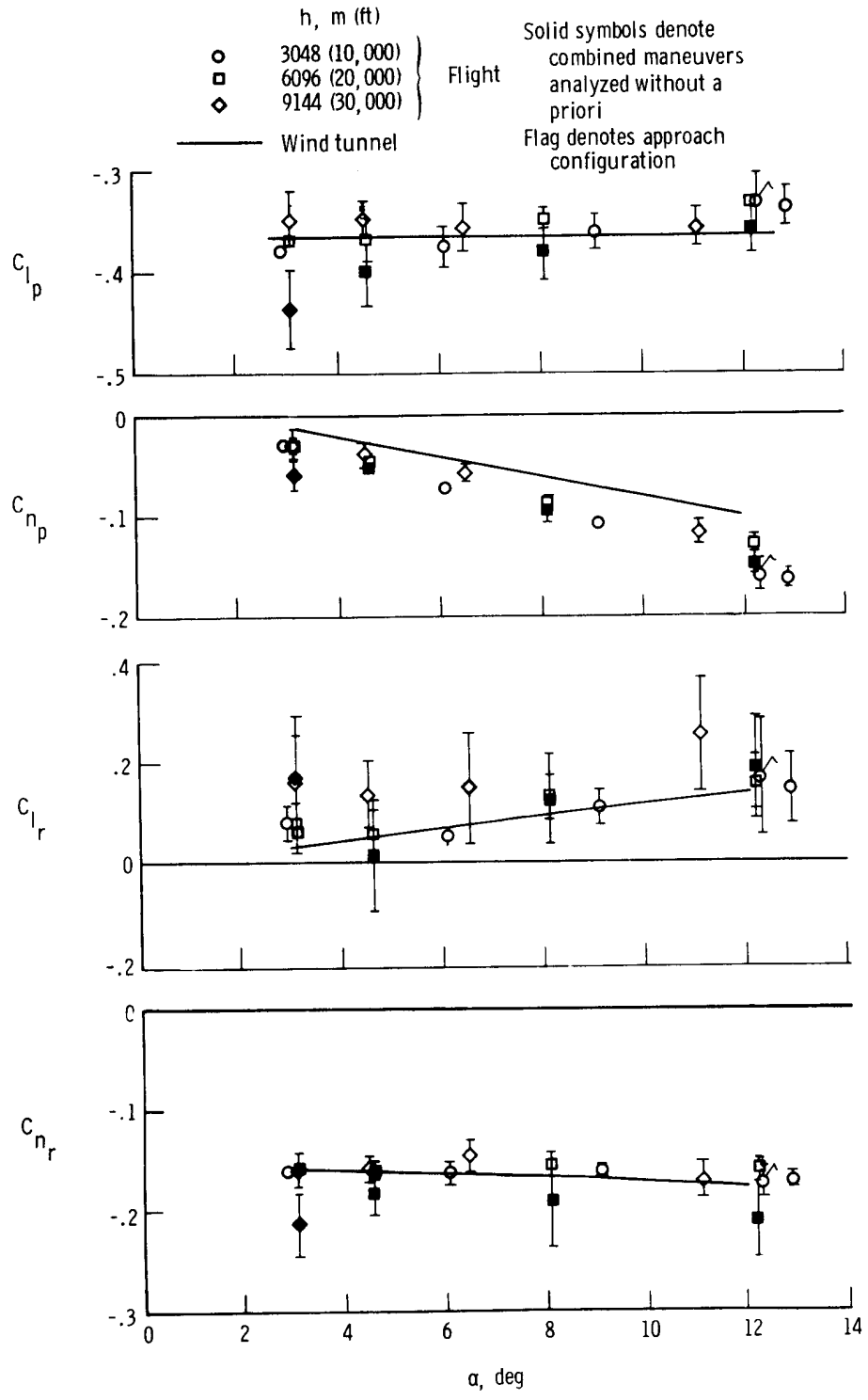

(d) Rotary derivatives.

Figure 5. Concluded.

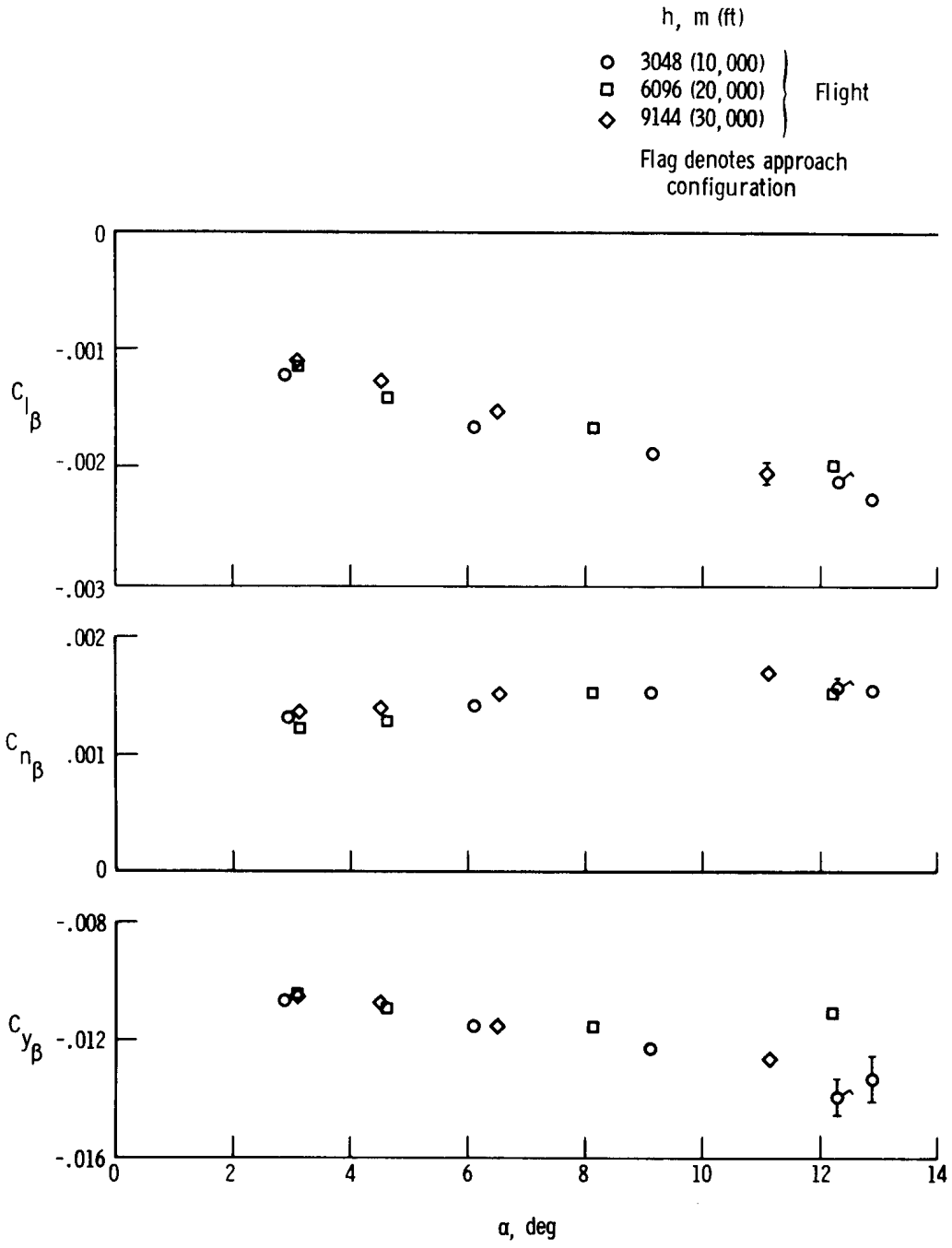

Figure 6. Final estimates of β derivatives determined from rudder maneuvers only.

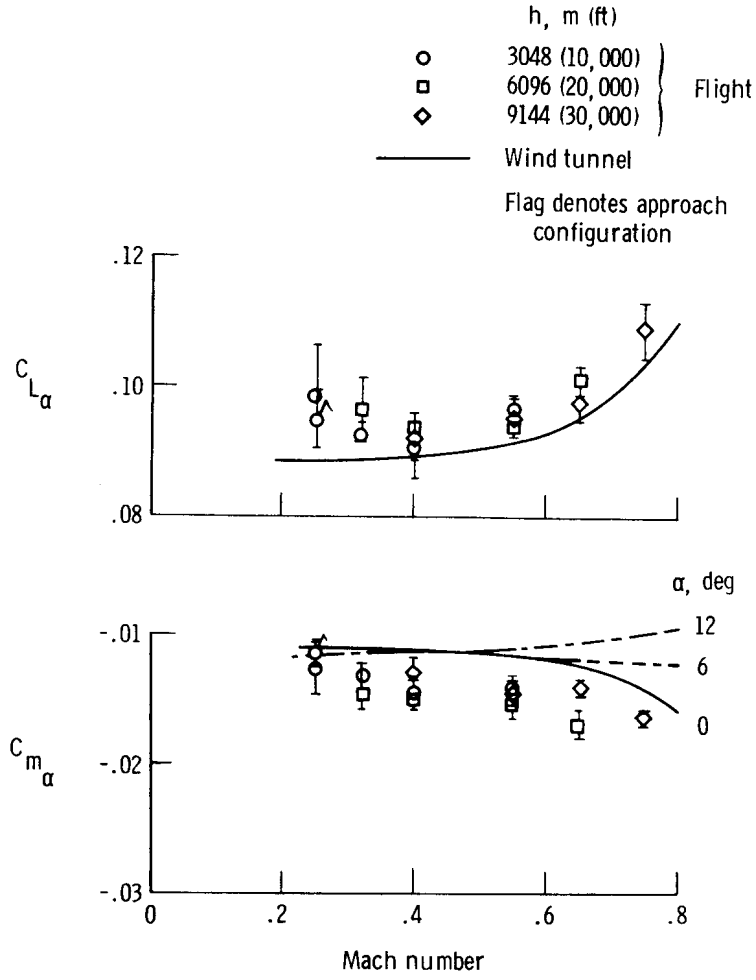

(a) α derivatives.

Figure 7. Longitudinal stability and control derivatives of the JetStar airplane obtained from flight by using the MMLE method.

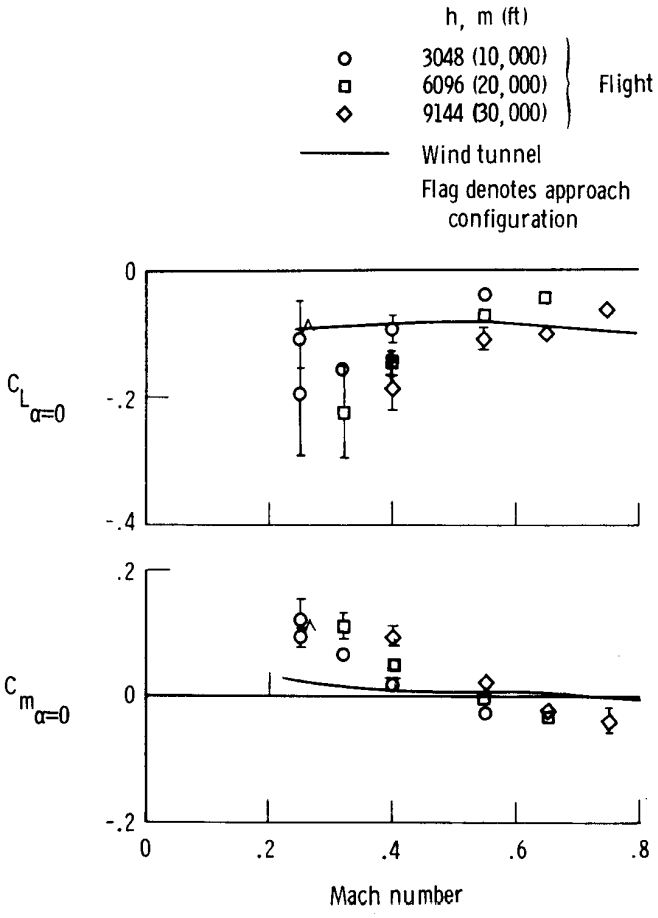

(b) Lift and pitching moment, $\alpha = 0$.

Figure 7. Continued.

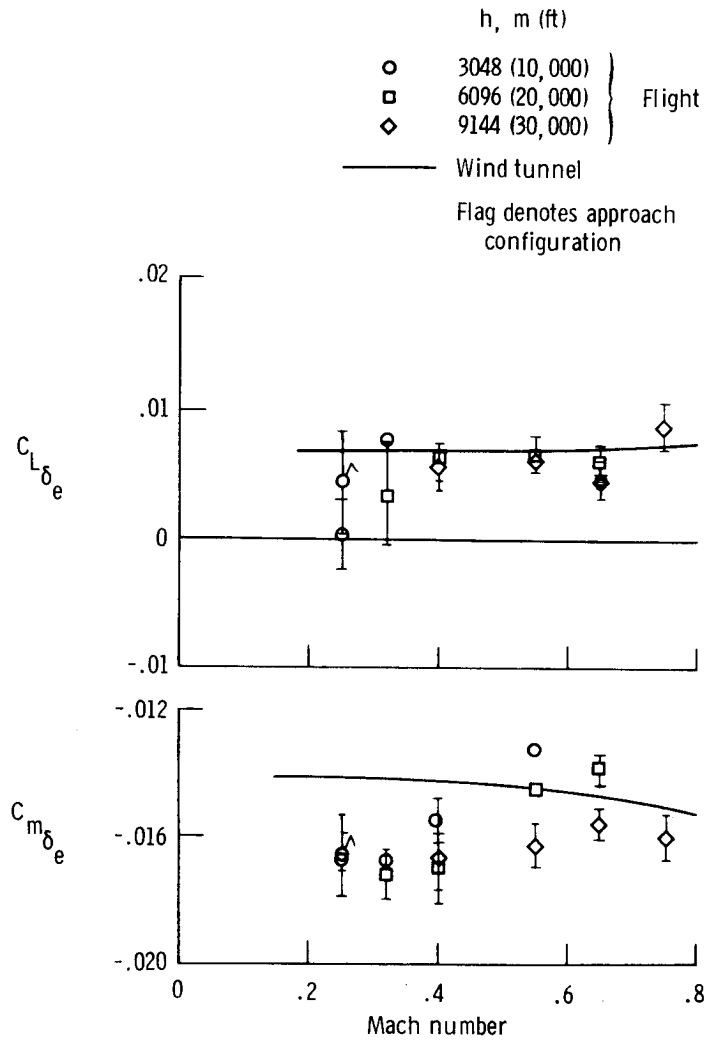

(c) δ_e derivatives.

Figure 7. Continued.

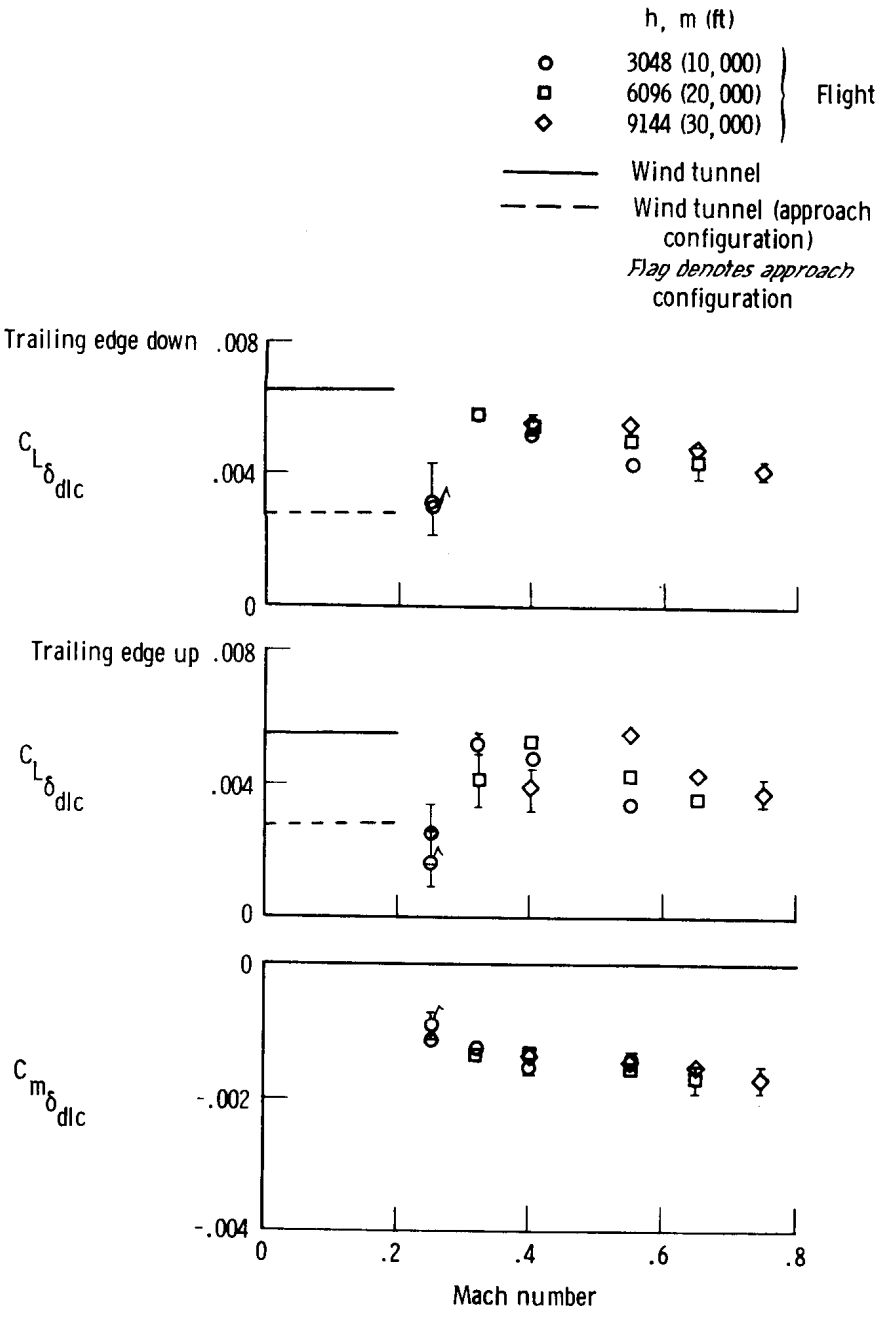

(d) Direct lift control derivatives.

Figure 7. Continued.

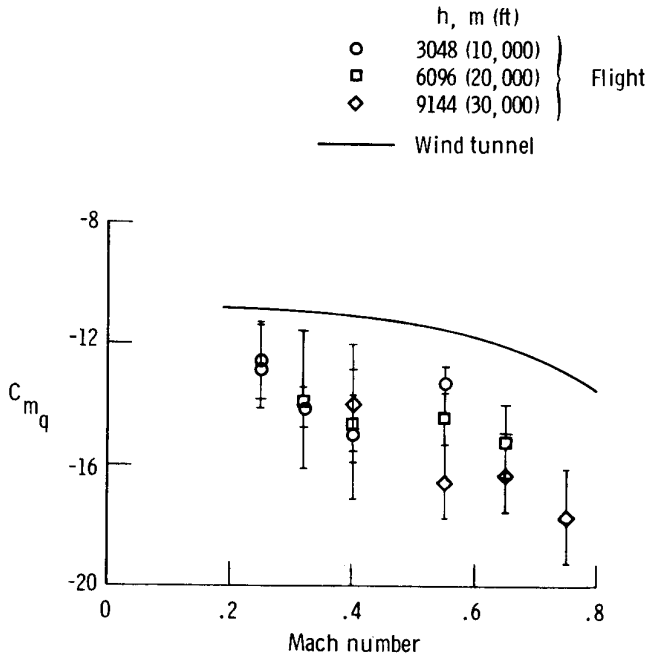

(e) C_{m_q} derivatives.

Figure 7. Concluded.

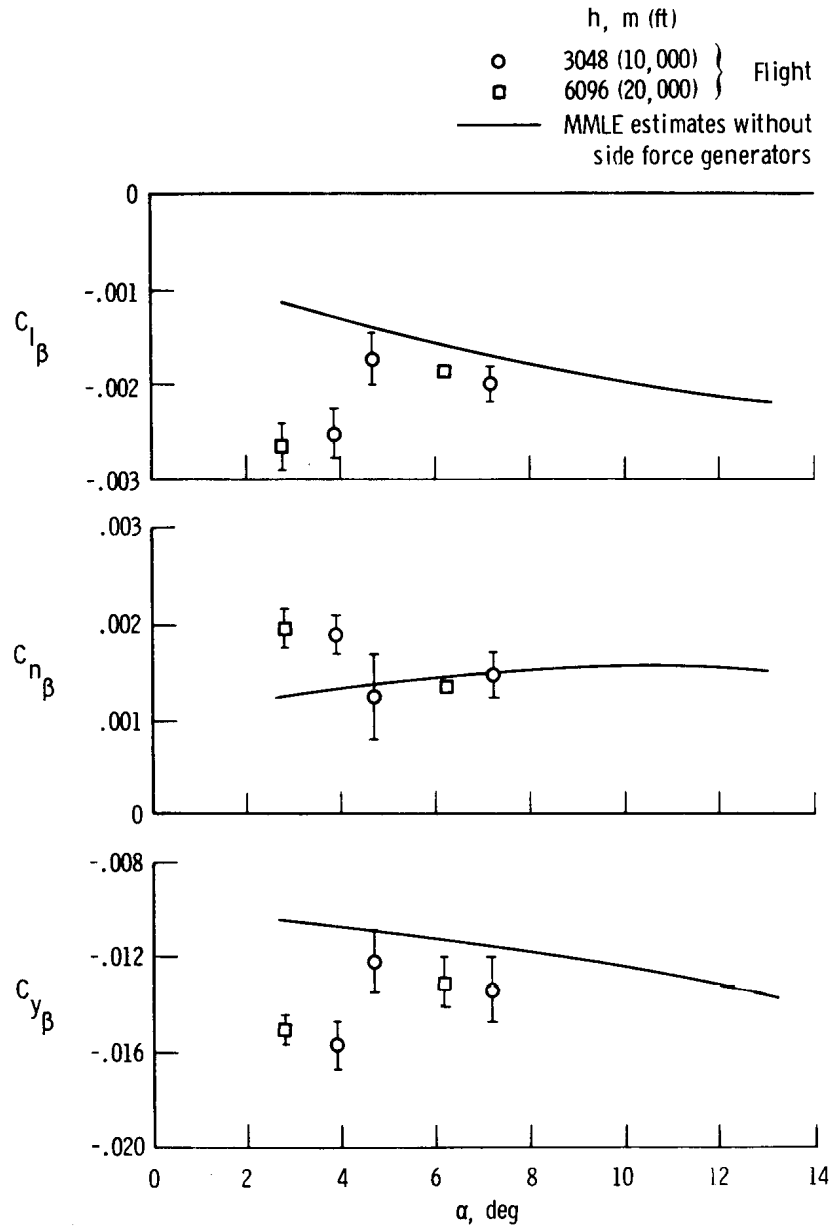

(a) β derivatives.

Figure 8. Effect of side force generators on lateral-directional stability and control derivatives.

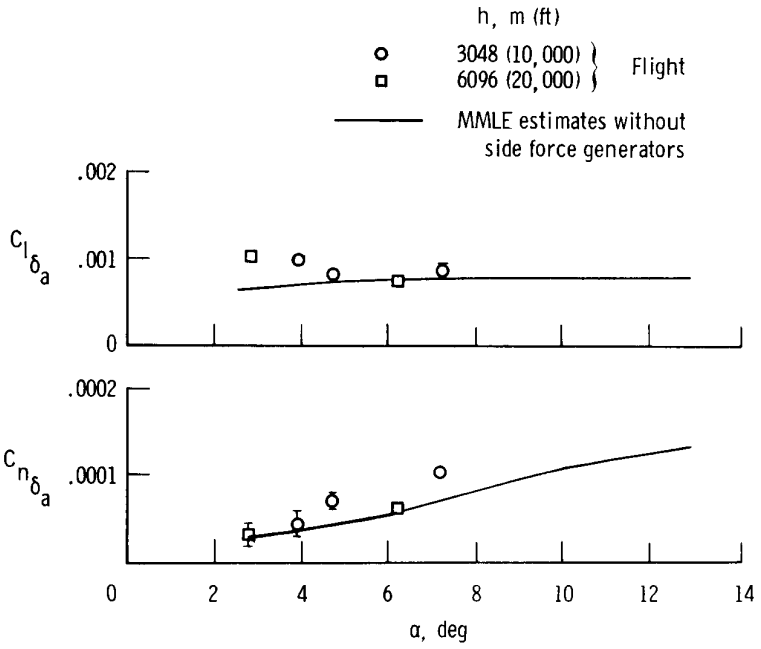

(b) δ_a derivatives.

Figure 8. Continued.

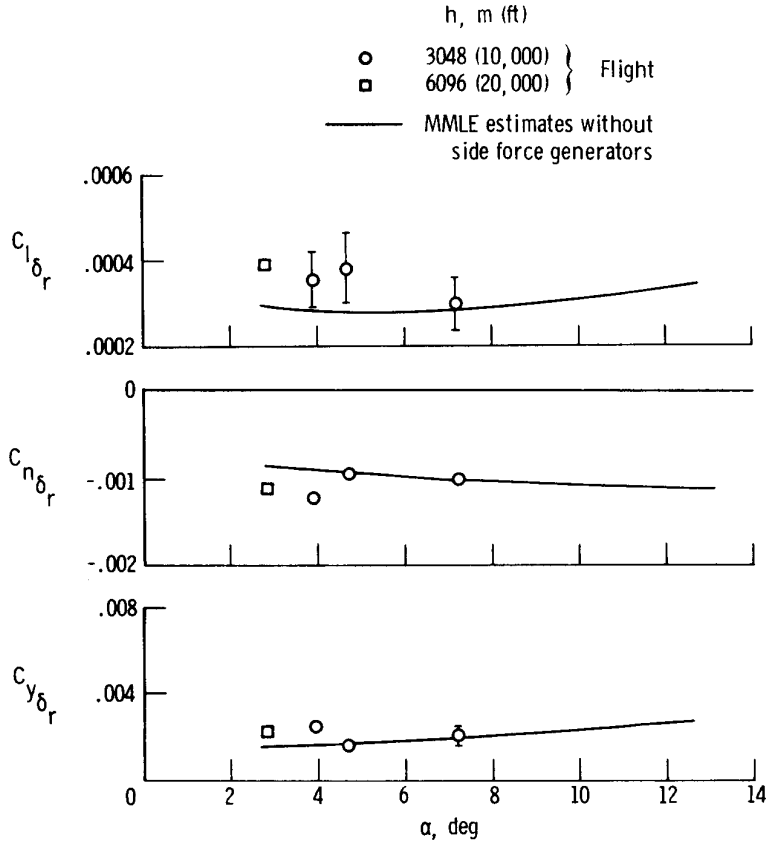

(c) δ_r derivatives.

Figure 8. Continued.

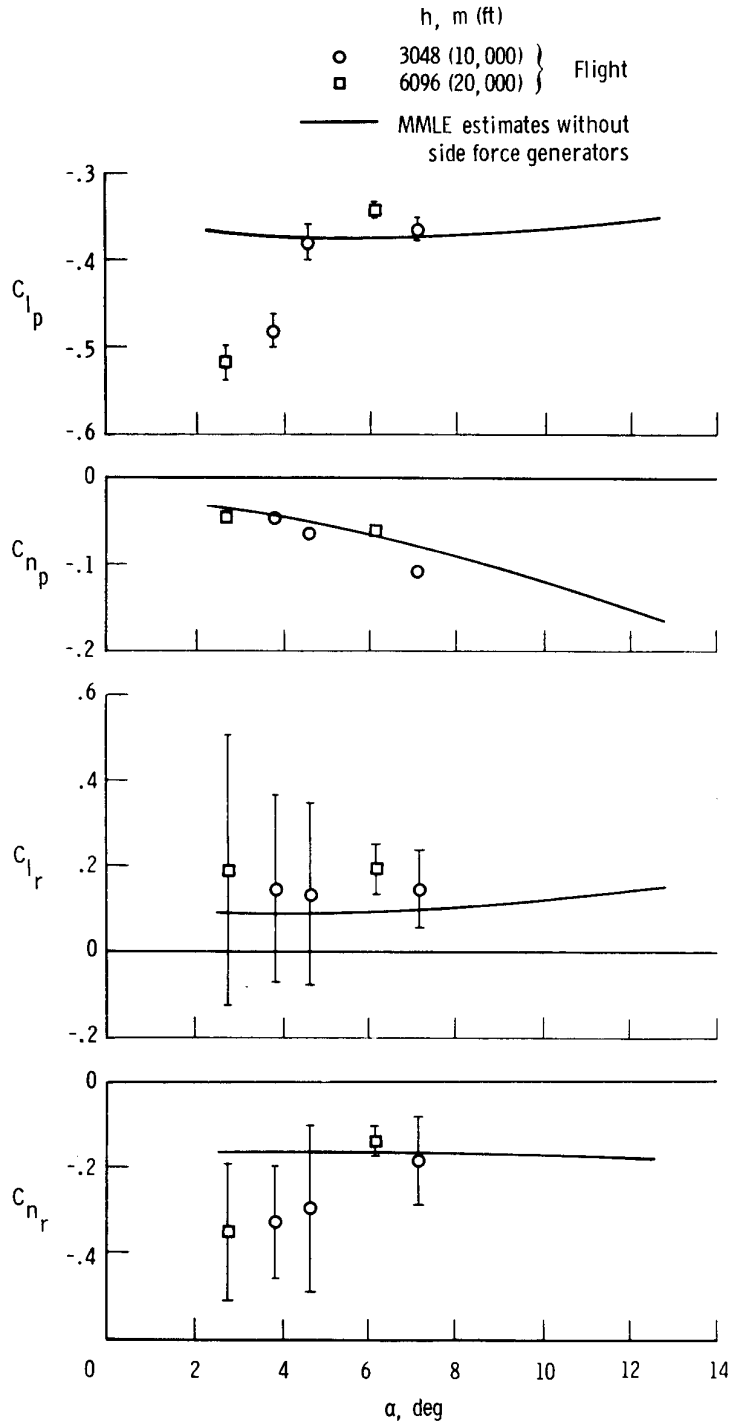

(d) Rotary derivatives.

Figure 8. Concluded.

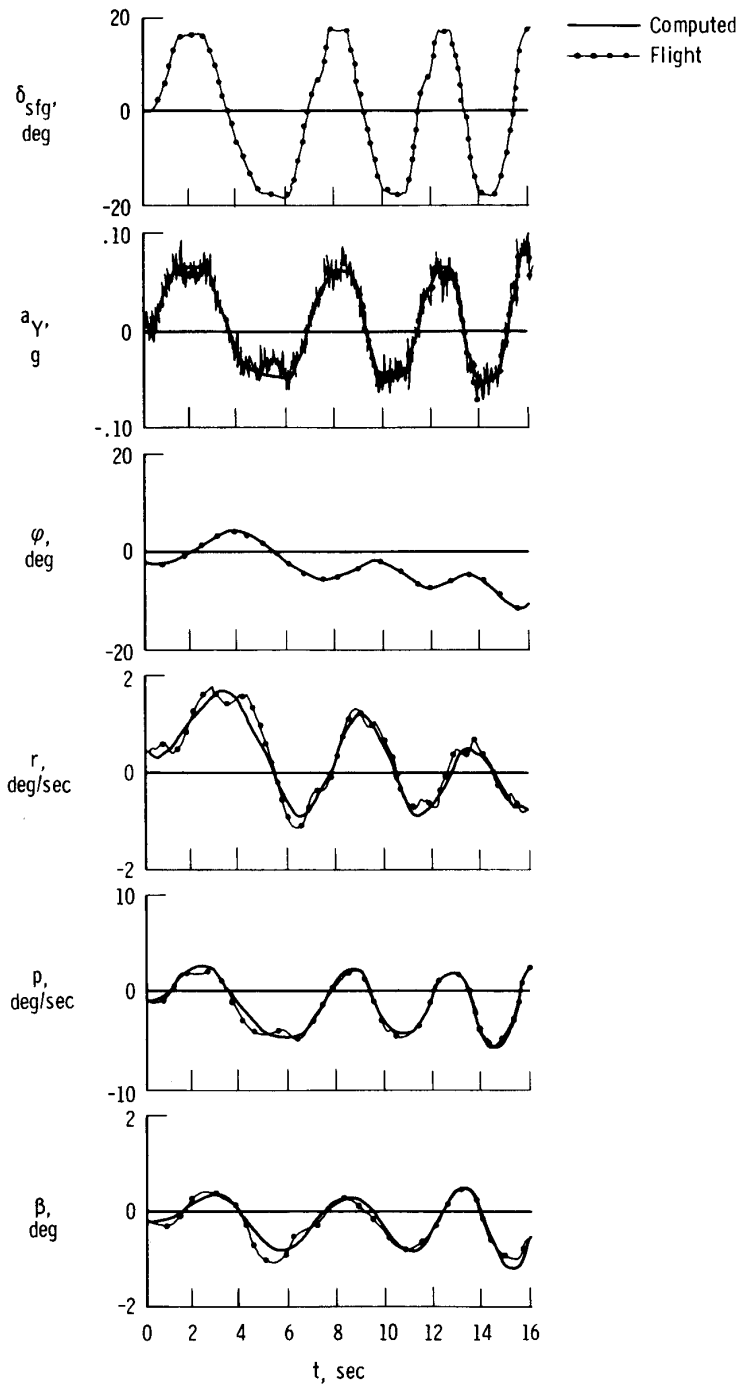

Figure 9. Time history of side force generator pulses.

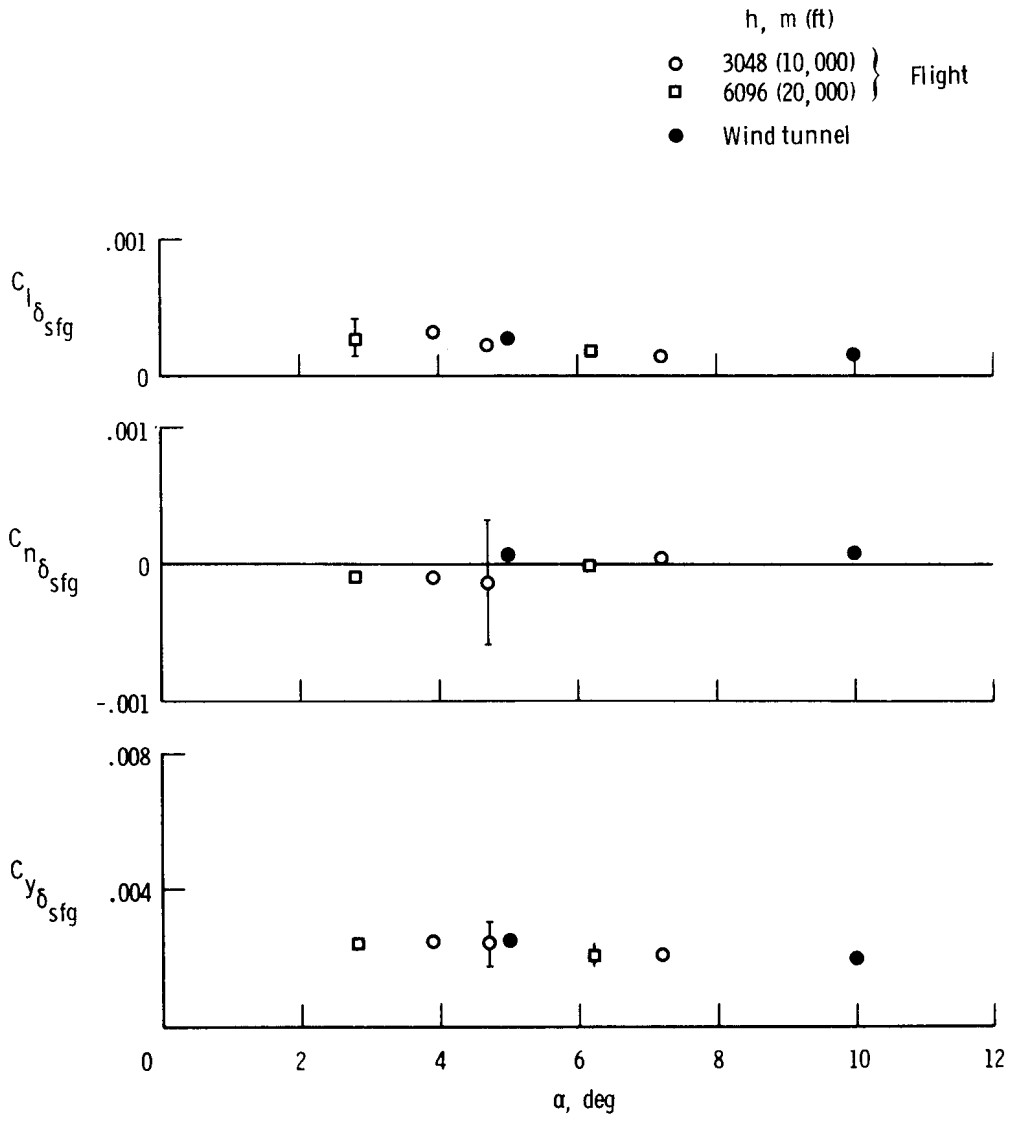

Figure 10. Side force generator effectiveness.